Fusion Engineering and Design 88 (2013) 8–16

Contents lists available at SciVerse ScienceDirect

Fusion Engineering and Design

journal homepage: www.elsevier.com/locate/fusengdes

Failure initiation and propagation of Li_4SiO_4 pebbles in fusion blankets

Shuo Zhao [a,b,*], Yixiang Gan [c], Marc Kamlah [b]

[a] College of Mechanical and Electronic Engineering, Hebei University of Science and Technology, Shijiazhuang, Hebei 050018, China
[b] Institute for Applied Materials, Karlsruhe Institute of Technology, D-76344 Eggenstein-Leopoldshafen, Germany
[c] Particles and Grains Laboratory, School of Civil Engineering, The University of Sydney, NSW 2006, Australia

ARTICLE INFO

Article history:
Received 7 March 2012
Received in revised form 4 June 2012
Accepted 17 September 2012
Available online 22 October 2012

Keywords:
Li_4SiO_4 pebbles
Critical energy
Failure
DEM simulation

ABSTRACT

Lithium orthosilicate (Li_4SiO_4) pebbles are considered to be a candidate as solid tritium breeder in the helium cooled pebble bed (HCPB) blanket. These ceramic pebbles might be crushed during thermomechanical loading in the blanket. In this work, the failure initiation and propagation of pebbles in pebble beds is investigated using the discrete element method (DEM). Pebbles are simplified as mono-sized elastic spheres. Every pebble has a contact strength in terms of critical strain energy, which is derived from a validated strength model and crush test data for pebbles from a specific batch of Li_4SiO_4 pebbles. Pebble beds are compressed uniaxially and triaxially in DEM simulations. When the strain energy absorbed by a pebble exceeds its critical energy it fails. The failure initiation is defined as a given small fraction of pebbles crushed. It is found that the load level for failure initiation can be very low. For example, if failure initiation is defined as soon as 0.02% of the pebbles have been crushed, the pressure required for uniaxial loading is about 2.5 MPa. Therefore, it is essential to study the influence of failure propagation on the macroscopic response of pebble beds. Thus a reduction ratio defined as the size ratio of a pebble before and after its failure is introduced. The macroscopic stress–strain relation is investigated with different reduction ratios. A typical stress plateau is found for a small reduction ratio.

© 2012 Elsevier B.V. All rights reserved.

1. Introduction

Pebble beds are integral parts of fusion reactors as solid breeder and neutron multiplier in the HCPB blanket [1,2]. The blanket contains two types of pebbles, ceramic breeder (lithium compound, such as Li_4SiO_4) and neutron multiplier (beryllium). During the operation of fusion reactors, pebbles will expand because of high temperatures in addition to thermal stresses introduced by the thermal mismatch between the pebble beds and container wall. This may lead to the failure of ceramic pebbles. It is foreseen that pebble failure will affect the overall thermomechanical response of pebble beds [3]. Therefore, the knowledge of pebble failure initiation and propagation in pebble beds is necessary for a safe and reliable design of the HCPB blanket.

The discrete element method (DEM) [4] is suitable to compute the motion of a large number of particles constituting a granular material, such as a pebble bed. This method has been already used to investigate the mechanical or thermal response of pebble beds for non-crushable pebbles [5–9]. For example, An et al. [5] show that packing factor (PF) and bed geometry have an impact on the mechanical stiffness of pebble beds. The packing factor is the ratio of the volume of all pebbles to the volume of the particle assembly, i.e., pebble bed. The significant influence of the PF can also be seen using periodic boundary conditions [7]. Thermomechanical properties of pebble beds, such as thermal stress or creep due to thermal expansion or external pressure, have been investigated by DEM as well [6,8,9]. On the other hand, particle failure can be taken into account into the DEM method as long as the particle strength can be quantitatively described and imported into DEM. For example, Marketos and Bolton [10] assume that particles will fail if the maximum contact force exerted on them exceeds a critical value. In their DEM simulations, pebbles are removed once they are crushed. In the research activities related to fusion engineering, although there are some papers concerning the strength of single pebbles [11–13], no work has been reported on the influence of pebble failure on the overall response of pebble beds.

In this work, we will include the pebble–pebble contact strength into DEM to study pebble failure initiation and propagation. For this purpose, we employ the pebble strength formulated in terms of strain energy, as it has been derived from a verified strength model [13]. This approach relies on experimental data. We will first focus on the load levels for the initiation of pebble failure under different loading conditions. For the identification of this load level, two different methods are used. In order to simulate the propagation of pebble failure, a reduction ratio of pebble size is introduced to characterize the presence of crushed pebbles. We discuss in detail

* Corresponding author at: College of Mechanical and Electronic Engineering, Hebei University of Science and Technology, Shijiazhuang, Hebei 050018, China. Tel.: +86 311 8166 8630; fax: +86 311 8166 8630.
E-mail addresses: shuo.zhao@hebust.edu.cn, vaselago@gmail.com (S. Zhao).

0920-3796/$ – see front matter © 2012 Elsevier B.V. All rights reserved.
http://dx.doi.org/10.1016/j.fusengdes.2012.09.008

the influence of pebble failure on the overall response of pebble beds.

This paper is organized as follows. The DEM code and pebble contact strength used in this work will be introduced in Section 2. Two methods identifying the load level for failure initiation are shown in Section 3. The influence of pebble failure propagation on the overall response of pebble beds will be presented in Section 4. Finally, conclusions are made in Section 5.

2. Simulation methods

2.1. Discrete element method

The DEM code developed at Karlsruhe Institute of Technology (KIT) will be used here [7]. The normal and tangential contact forces are calculated from Hertz contact theory and a linear friction model, respectively. A separate code provides a random initial configuration, namely the positions of the centers of the mono-sized spherical particles, at a prescribed packing factor, such that there is no overlapping of any particles in the assembly [7]. Periodic boundary conditions are employed, by which only a comparably small number of particles in a representative volume element (RVE) is needed to obtain statistical information on the bulk behavior of a pebble bed. In this way, this boundary condition leads to a limitation of the computational efforts for simulations.

In this work, a periodic assembly of 5000 spheres in a cubic box is considered which is subject to periodic boundary conditions. The edge length of the box is about 8 mm. In view of Li_4SiO_4 pebbles for fusion breeding blanket applications, Young's modulus and Poisson's ratio of the spheres are chosen as $E = 90$ GPa and $\nu = 0.25$ [12], respectively. The spheres have a size of 0.5 mm which is the mean size of Li_4SiO_4 pebbles from the batch OSi 07/1 produced for breeding blanket applications [13,14]. The friction coefficient is set to $\mu = 0.1$ unless otherwise specified. The shear stiffness in the friction model is $16G^*/3$ where $G^* = 55$ GPa is the equivalent shear modulus for Li_4SiO_4 pebbles [13]. Uniaxial and triaxial load, respectively, will be applied under displacement control on the pebble beds. As mentioned before, we focus on the load level for failure initiation and on the macroscopic stress–strain relation along with failure propagation.

2.2. Pebble strength

According to the strength model adopted in this work, a pebble fails if the strain energy absorbed by it reaches a critical level. For the case of the Li_4SiO_4 pebbles considered in this work, this criterion has been developed, verified and discussed in full detail in [13,15]. The probability density function (PDF) of the contact strength, i.e., critical strain energy of pebbles, is given by

$$p_s(W_c) = \frac{m}{W_{Mat}}\left(\frac{W_c}{W_{Mat}}\right)^{m-1}\exp\left(-\left(\frac{W_c}{W_{Mat}}\right)^{m}\right), \quad (1)$$

where W_c is the critical strain energy, m and W_{Mat} are material parameters. For these material parameters, the values $m = 3.2$ and $W_{Mat} = 8.2 \times 10^{-6}$ J, have been identified for pebbles with a diameter of 0.5 mm from the mentioned batch OSi 07/1 under fusion relevant conditions, that is, the pebbles were subjected to high temperature and dry inert gas. In DEM simulations, a critical energy is distributed randomly among pebbles according to Eq. (1). The method to assign the critical energy to each pebble will be given later in Section 3.2.

We recall, that a pebble will fail if the strain energy it has actually absorbed exceeds its individual critical energy. Assuming that there is no interaction between different contact areas of a pebble, the strain energy for pebbles in pebble beds can be calculated by

$$W_a = \sum_{i=1}^{N_c} cF_i^{5/3}, \quad (2)$$

where N_c is the coordination number, i.e., the number of contacts, of the pebble, F_i is the contact force of ith contact($i = 1, 2, \ldots, N_c$), and c is a constant derived from Hertz theory given by

$$c = \frac{1}{5}\left(\frac{9}{16R^*}\right)^{1/3}\frac{1}{E^{*(2/3)}}. \quad (3)$$

Here, R^* is the relative radius of curvature, and E^* is the equivalent Young's modulus. For a contact between mono-sized spherical pebbles, $R^* = R/2$ and $E^* = E/(2(1-\nu^2))$, where R, E and ν are the radius, Young's modulus and Poisson's ratio of pebbles, respectively.

3. Prediction of failure initiation in a pebble bed

In this section we will introduce two approaches for the prediction of the initiation of pebble failure in a pebble bed. The first method relies not only on numerical simulations based on DEM but also analytical analysis, while the second one is completely numerical. Furthermore, both methods will be discussed and compared.

3.1. Numerical-analytical method

The basic assumption of the first method is that the distribution of the actual strain energy absorbed by pebbles and the distribution of the strength of single pebbles in terms of critical strain energy are two independent events. Furthermore, we assume that both events are not affected by the failure of pebbles, which seems to be acceptable as long as only a small number of pebbles have failed in the pebble bed.

For the case that the failure of spheres would be dominated by the maximum contact force, the failure probability of all spheres, i.e., the number of crushed spheres divided by the number of all spheres, has been derived by [10]

$$P_f = \int_{F_{min}}^{F_{max}} p_s(F = \Phi)\tilde{P}(F > \Phi)d\Phi, \quad (4)$$

where the integration variable Φ represents the critical contact force, while F_{min} and F_{max} are the minimum and maximum contact strength (critical contact force) for the spheres which are given arbitrarily in their DEM simulations. $p_s(\Phi)$ or $p_s(F = \Phi)$ is the PDF of the contact strength. The notation $\tilde{P}(F > \Phi)$ means the probability of the maximum contact force exerted on a sphere being larger than Φ. For continuous distributions, $\tilde{P}(F > \Phi) = \int_{\Phi}^{\infty} p(\Phi)d\Phi$ where $p(\Phi)$ is the PDF of the maximum contact force on every sphere obtained in DEM simulations.

Eq. (4) can be adopted for other strength models, such as the critical energy distribution in our case, giving

$$\begin{aligned} P_f &= \int_{W_{cmin}}^{W_{cmax}} p_s(W_c = \Phi)\tilde{P}_e(W_a > \Phi)d\Phi \\ &= \int_{W_{cmin}}^{W_{cmax}} p_s(\Phi)(1 - P_e(\Phi))d\Phi, \end{aligned} \quad (5)$$

where the integration variable Φ now represents the critical energy of pebbles, W_{cmin} and W_{cmax} are the minimum and maximum critical energy for pebbles, $p_e(\Phi)$ and $P_e(\Phi)$ are the PDF and the cumulative density function (CDF), respectively, with respect to the absorbed strain energy W_a in pebble beds. Similar to $\tilde{P}(F > \Phi)$, $\tilde{P}_e(W_a > \Phi)$ means the probability of the strain energy absorbed by

every sphere being larger than Φ. The failure probability can also be written as

$$P_f = \int_{W_{amin}}^{W_{amax}} \tilde{P}_s(W_c < \Phi) p_e(W_a = \Phi) d\Phi = \int_{W_{amin}}^{W_{amax}} P_s(\Phi) p_e(\Phi) d\Phi. \quad (6)$$

Here, W_{amin} and W_{amax} are the minimum and maximum strain energy absorbed by pebbles. The notation $\tilde{P}_s(W_c < \Phi)$ means the probability of the pebble strength being smaller than Φ. For continuous distributions, $\tilde{P}_s(W_c < \Phi) = P_s(\Phi) = \int_{-\infty}^{\Phi} p_s(\Phi) d\Phi$. Note that the CDF, e.g., $P_s(x = \Phi)$ or $P_s(\Phi)$, is conventionally defined as the probability of the random variable x not being bigger than the real number Φ, that is, $\tilde{P}_s(x \leqslant \Phi)$. According to this definition, the equation $P_s(W_c = \Phi) = \tilde{P}_s(W_c < \Phi)$ used in Eq. (6) might not hold especially for discrete distributions. Moreover, both (5) and (6) may have to be replaced by a summation of the kind $\sum_i p_s(W_c = \Phi_i)\tilde{P}_e(W_a > \Phi_i)$ or $\sum_i \tilde{P}_s(W_c < \Phi_i) p_e(W_a = \Phi_i)$ for discrete distributions where Φ_i is the ith point of discontinuity of the discrete distribution. However, $\tilde{P}_s(W_c \leqslant \Phi) = \tilde{P}_s(W_c < \Phi)$ will always hold for continuous distributions, such as Eq. (1) in our case, since the probability of any specified strength Φ is zero, that is, $\tilde{P}(W_c = \Phi) \equiv 0$.

The physical meaning of Eq. (5) is that for a given critical energy, namely W_c, the pebbles with an absorbed strain energy larger than W_c, i.e., $W_a > W_c$, will fail. The physical meaning of Eq. (6) is that for a given strain energy, namely W_a, the pebbles with a critical energy less than W_a, i.e., $W_c < W_a$, will fail. In fact, both equations describe the same event. Moreover, it can be seen from both equations that pebbles will not fail in the critical case, that is, $W_a = W_c$. If one considers the pebble will fail at the critical case, Eqs. (5) and (6) have to be slightly modified, i.e., $\tilde{P}_e(W_a \geqslant \Phi)$ instead of $\tilde{P}_e(W_a > \Phi)$ in Eq. (5) and $\tilde{P}_s(W_c \leqslant \Phi)$ instead of $\tilde{P}_s(W_c < \Phi)$ in Eq. (6). For continuous distributions, it makes no difference whether to consider the critical case or not. For discrete distributions, the probability at the points of discontinuity might not be zero and consequently $\tilde{P}_e(W_a \geqslant \Phi) \neq \tilde{P}_e(W_a > \Phi)$ and $\tilde{P}_s(W_c \leqslant \Phi) \neq \tilde{P}_s(W_c < \Phi)$, which indicates the significance of the critical case. In the critical case, namely $W_a = W_c$, pebbles will fail or survive depending on our definition.

It needs to be noted that there are necessary conditions for Eqs. (5) and (6), namely

$$\int_{W_{cmin}}^{W_{cmax}} p_s(\Phi) d\Phi = 1 \quad \text{and} \quad \int_{W_{amin}}^{W_{amax}} p_e(\Phi) d\Phi = 1. \quad (7)$$

The minimum critical energy W_{cmin} has to be a positive value in view of its physical meaning. For theoretical analysis, $p_s(\Phi)$ and corresponding W_{cmin} and W_{cmax} satisfying Eq. (7) can be prescribed arbitrarily, e.g., Eq. (3) in the paper [10]. For practical application like our case, the distribution $p_s(\Phi)$ may be derived from experimental data by fitting. There are two points in the course of deriving $p_s(\Phi)$.

First, crush experiments should be carried out on pebbles which are statistically the same in the aspect of size, shape, batch, under the same environment, etc. The variation of the crush loads for the pebbles arises from the random existence of natural flaws in them. As a consequence of random size and position of the natural flaws, the pebble strength will be a continuous distribution in principle. It will be reasonable to use a continuous fitting function of $p_s(\Phi)$. The fitting function can be any kind of reasonable distributions, such as a Weibull distribution.

Second, either all the parameters or part of them in the fitting function can be obtained from experimental data. For the former case, if there is no default value of W_{cmin}, unlike in Eq. (1) where

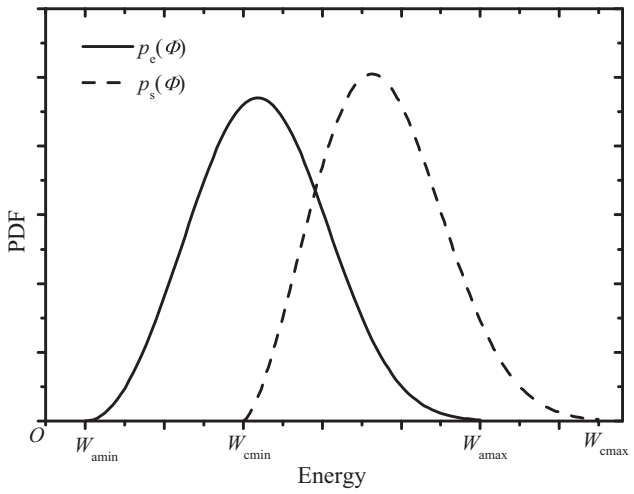

Fig. 1. An example of continuous p_s and p_e where $\tilde{P}_s(\Phi < W_{cmin}) = \tilde{P}_e(\Phi < W_{amin}) = \tilde{P}_s(\Phi > W_{cmax}) = \tilde{P}_e(\Phi > W_{amax}) = 0$.

$W_{cmin} = 0$ is default, W_{cmin} will be one of the fitting parameters. It is possible, from the mathematical point of view, that the fitting parameter W_{cmin} is smaller than 0. If so, there would exist a negative strength which is physically impossible. Therefore, the fitting function of p_s has to be carefully chosen so that the resultant W_{cmin} will be not smaller than zero. In case only part of the parameters are fitted, one or more parameters are prescribed in order to avoid physically impossible values like $W_{cmin} < 0$. One can consider setting the W_{cmin} to be the one corresponding to the minimum crush load found in crush tests. The distribution of $p_e(\Phi)$ has to be derived from DEM simulations. In particular, the probability $\tilde{P}_e(\Phi \leqslant 0)$ can be larger than zero, which means there might exist some spheres having no contact with others.

For continuous distributions, an example of possible $p_s(\Phi)$ and $p_e(\Phi)$ is shown in Fig. 1. It can be seen from this figure that the interval in both Eqs. (5) and (6) can be reduced to $[W_{min}, W_{max}] = [W_{cmin}, W_{cmax}] \cap [W_{amin}, W_{amax}]$ in view of $\tilde{P}_s(\Phi < W_{cmin}) = \tilde{P}_e(\Phi < W_{amin}) = \tilde{P}_s(\Phi > W_{cmax}) = \tilde{P}_e(\Phi > W_{amax}) = 0$. Since W_{cmin} is a non-negative parameter in view of its physical meaning, W_{min} is a non-negative value as well. If the intersection $[W_{min}, W_{max}]$ is an empty set, the failure probability P_f is either 0, i.e., for $W_{amax} < W_{cmin}$, or 1, i.e., for $W_{amin} > W_{cmax}$. For discrete distributions containing points of discontinuity at which the probability is not equal to zero, we would have to define whether the pebble will fail in the critical case as previously mentioned.

However, in our case we have taken a continuous $p_s(\Phi)$. We will also consider a continuous $p_e(\Phi)$, to be specific, in the form of a three parameter Weibull distribution, and consequently we do not need to discuss the situation of the critical case when $W_a = W_c$. The parameters of $p_e(\Phi)$ will be determined by fit of strain energy distributions.

Neglecting pebble failure during loading, the strain energy distribution among pebbles can be obtained from DEM simulations. Fig. 2 shows the strain energy distribution P_e in one assembly (PF = 64.141%) for different load levels subjected to uniaxial strain loading, i.e., $\varepsilon_x = \varepsilon_y = 0$, $\varepsilon_z < 0$. The energy is normalized by W_n corresponding to the strain energy absorbed by a pair of contacting pebbles subjected to a normal load of F_{ave} given by

$$W_n = 2cF_{ave}^{5/3}. \quad (8)$$

Here, F_{ave} is the mean value of all normal contact forces present in the particle assembly, and c is defined in Eq. (3). It becomes obvious that there is a master curve representing all load levels for the considered PF = 64.141%. For uniaxial loading this master curve has

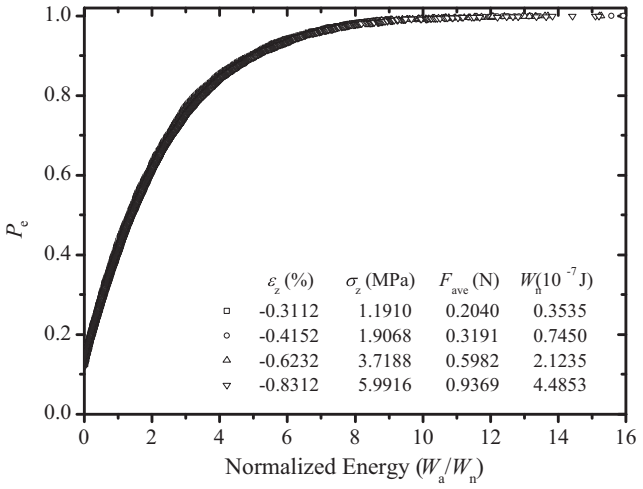

Fig. 2. Normalized strain energy distribution P_e under different load levels for uniaxial loading. Negative strain stands for compression. The different markers correspond to increasing levels of prescribed uniaxial macroscopic strain.

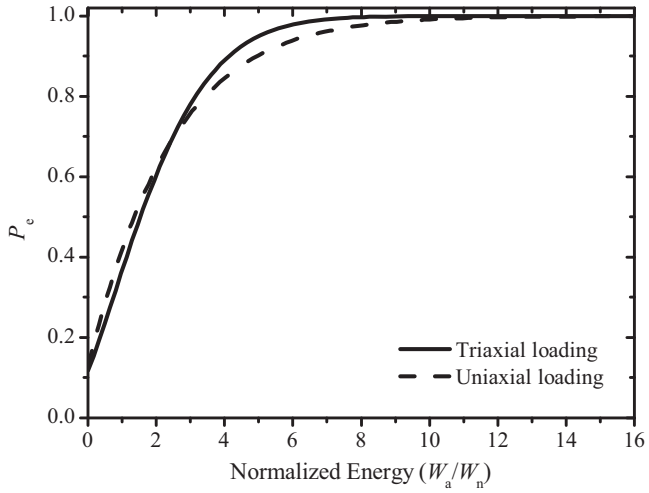

Fig. 4. Fitting curves for normalized strain energy distribution P_e for uniaxial and triaxial loading.

been confirmed for further load levels, and even for other PFs. Two cases for other PFs are shown in Fig. 3. The probability at $W_a = 0$ is approximately 0.12, meaning that about 12% pebbles have no contacts at all during loading. This is possible since gravity is not taken into account. For triaxial loading, i.e., $\varepsilon_x = \varepsilon_y = \varepsilon_z < 0$, there exists a master curve as well, however it is different from the one for uniaxial loading. Both master curves are fitted by a three parameter Weibull distribution, that is,

$$P(x) = 1 - \exp\left(-\left(\frac{x-b}{a}\right)^m\right), \tag{9}$$

where a, b and m are fitting parameters, and the variable x corresponds to W_a/W_n. The fitting parameters are $a = 2.46$, $b = -0.398$, and $m = 1.08$ for uniaxial loading and $a = 2.94$, $b = -0.809$, and $m = 1.61$ for triaxial loading, respectively. Fig. 4 shows the corresponding fitting curves.

Care should be taken that the fitting function is not the CDF of $P_e(\Phi)$ unless the fitting parameter b is not smaller than zero. If $b \geqslant 0$, b corresponds to the minimum strain energy W_{amin}. However, in our case b is smaller than zero. If we take the fitting functions as the $P_e(\Phi)$, there would exist the possibility of negative strain energy which is physically impossible. Alternatively, we can define the $P_e(\Phi)$ based on the fitting functions as

$$P_e(\Phi) = \begin{cases} 1 - \exp\left(-\left(\dfrac{\Phi + 0.398}{2.46}\right)^{1.08}\right) & \Phi \geqslant 0 \\ 0 & \Phi < 0 \end{cases} \quad \text{for uniaxial loading,} \tag{10}$$

$$P_e(\Phi) = \begin{cases} 1 - \exp\left(-\left(\dfrac{\Phi + 0.809}{2.94}\right)^{1.61}\right) & \Phi \geqslant 0 \\ 0 & \Phi < 0 \end{cases} \quad \text{for triaxial loading,} \tag{11}$$

where the normalized energy Φ corresponds to W_a/W_n. Such definitions of P_e mean the minimum strain energy W_{amin} is zero. The interval for both distributions in Eqs. (11) and (10) is $[W_{amin}, W_{amax}] = [0, \infty]$. Eqs. (11) and (10) are non-continuous CDFs. At the point of discontinuity $\Phi = 0$ we define that pebbles having no strain energy will not fail no matter what the strength is.

Substitution of Eqs. (11) and (10), respectively, and (8), (1) into (5), where $[W_{cmin}, W_{cmax}] = [0, \infty]$, yields the failure probability P_f in terms of F_{ave} for uniaxial and triaxial loading. The results are shown in Fig. 5. Alternatively, the same results can be derived when substituting the PDFs corresponding to Eqs. (11) and (10) into (6), respectively. It should be noted that the failure probability

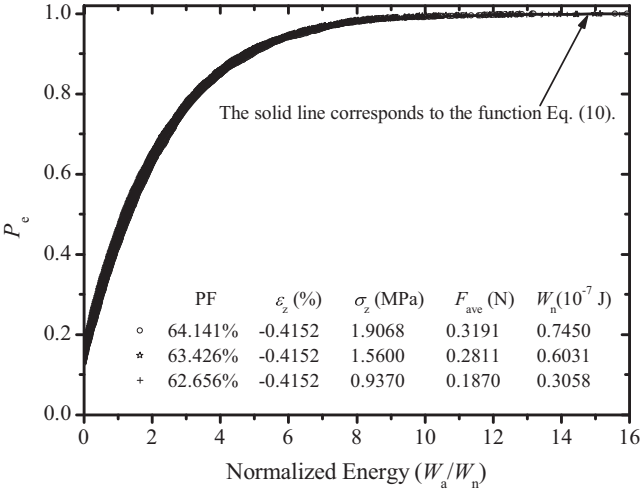

Fig. 3. Simulation results for various PFs shown in comparison to the same master curve as in Fig. 2.

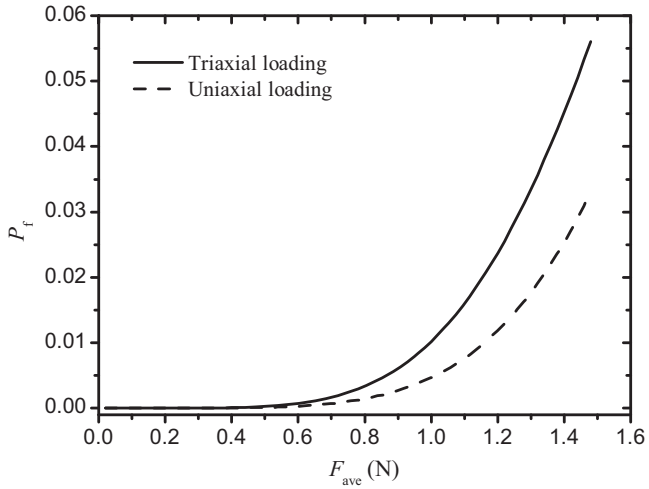

Fig. 5. Predicted failure probability P_f for pebbles from the batch OSi 07/1 in pebble beds.

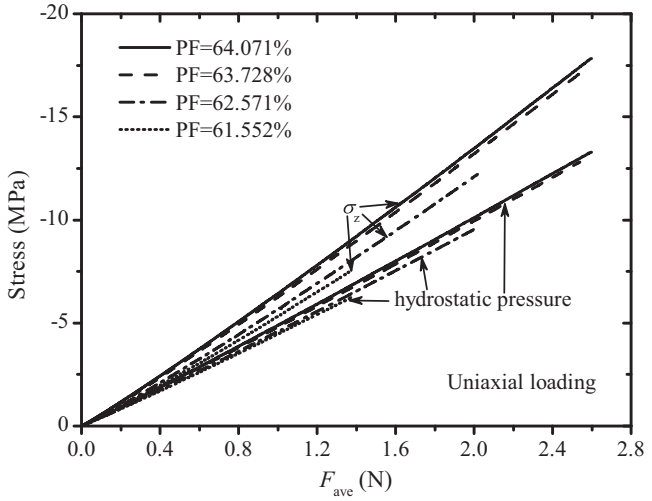

Fig. 6. The relation between average contact force and macroscopic stress σ_z along the loading axis and hydrostatic pressure for uniaxial loading.

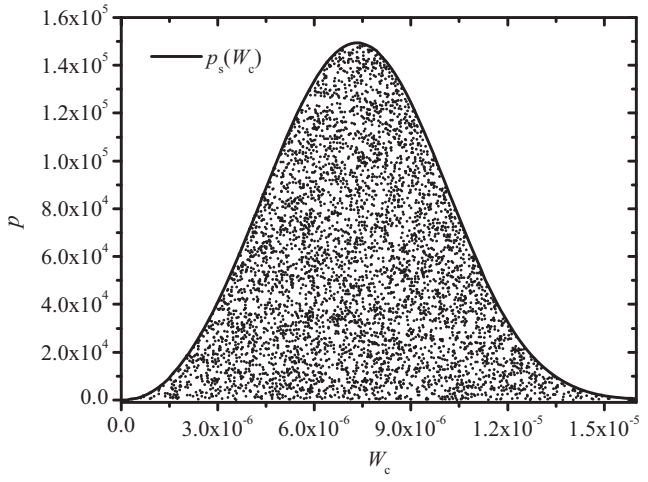

Fig. 7. Random numbers satisfying $p \leqslant p_s(W_c)$, where p_s is the PDF of the critical energy for pebbles.

P_f becomes unreliable with increasing F_{ave}, because the true distribution P_e will be modified by crushed pebbles.

The failure probability P_f in Fig. 5 can also be expressed in terms of macroscopic stresses, e.g., the macroscopic stress σ_z along the loading direction or the hydrostatic pressure. Fig. 6 shows the relations between F_{ave} and σ_z as well as the relations between F_{ave} and hydrostatic pressure for some PFs computed for uniaxial loading under the assumption that no pebbles will fail. In both cases, the relation obviously depends on the PF. As a result, the relation between P_f and σ_z or hydrostatic pressure will be dependent on PF.

The method presented in this subsection is based on numerical results, such as Figs. 4 and 6, and analytical analysis, such as Eqs. (5) or (6) as well as the experimental results, such as Eq. (1). The strain energy distribution P_e or p_e depends on the loading method (see Fig. 4) and is independent of PF as previously mentioned. For both uniaxial and triaxial loading methods, it is further found that the strain energy distribution only depends on the internal parameter F_{ave}. Thus, the failure probability P_f is preferred to be expressed in terms of F_{ave}, i.e., $P_f(F_{ave})$ in Fig. 5, rather than of macroscopic stresses and PF, i.e., $P_f(\sigma, PF)$. In order to make use of the prediction of $P_f(F_{ave})$ for practical application, first we need to know the loading method and initial PF of pebble beds before any loading. Second we compute the corresponding F_{ave} under a given macroscopic stress which can be measured. Finally, the failure probability can be predicted by the computed F_{ave} and $P_s(F_{ave})$.

3.2. Numerical method

We now introduce a second, purely numerical method for the prediction of failure initiation. We recall that any pebble in DEM simulations fails when $W_a > W_c$. For the implementation of the method, a critical energy W_c is prescribed to each pebble. To begin with, every pebble in the simulation, after having been picked randomly, is associated with a unique identification number (ID) such that we can record the information of the pebble during loading. As described in the following, a Monte Carlo method is used to assign to each pebble a critical energy such that the distribution of W_c-values among all pebbles is in agreement with the critical energy distribution p_s, i.e., Eq. (1).

A pair of statistically independent random numbers (W_c, p) is generated in the range of $0 \leqslant W_c \leqslant W_c^u$ and $0 \leqslant p \leqslant p_{max}$. In principle, the random number W_c should be generated in the range of $0 \leqslant W_c < \infty$. However, it is necessary to select an upper limit of W_c in the Monto Carlo method. An appropriate value for this upper limit W_c^u has to be selected such that $\int_0^{W_c^u} p_s(W_c)dW_c \approx 1$. In our case, this value was obtained as $W_c^u = 0.000016$, which corresponds to $\int_0^{W_c^u} p_s(W_c)dW_c = 0.9998$. The upper limit of the random number p in this method is, at least, larger than the maximum $p_s(W_c)$ for any possible W_c. In this work, we used $p_{max} = 160,000$. Care should be taken that the $p_s(W_c)$ depends on the batch of pebbles. The distribution $p_s(W_c)$ used in this work is derived for pebbles from the batch OSi 07/1 mentioned before.

From the pair (W_c, p) generated randomly in this way, if the value of p lies below the PDF, i.e., $p \leqslant p_s(W_c)$ holds, the first pebble (ID = 1) is assigned to the corresponding value of W_c as its critical energy. If $p > p_s(W_c)$, the corresponding pair (W_c, p) has to be discarded. Subsequently, we generate another pair of random numbers in the range $0 \leqslant W_c \leqslant W_c^u$ and $0 \leqslant p \leqslant p_{max}$, and W_c will be assigned to the second pebble (ID = 2) if $p \leqslant p_s(W_c)$. This procedure is repeated until every pebble has a prescribed critical energy. Fig. 7 shows 5000 pairs of (W_c, p) satisfying $p \leqslant p_s(W_c)$ together with $p_s(W_c)$. Both assignment of ID number and critical energy are two independent and random events. As a result, it can be regarded that a critical energy has been assigned to all pebbles, and the distribution of W_c for all pebbles will satisfy the distribution of the critical energy, i.e., Eq. (1), as in the example of Fig. 7.

We now define the initiation of failure in the pebble bed during a simulation as the instant or load level, when N_f pebbles have reached their critical energy. The number N_f of crushed pebbles can be computed from a prescribed failure probability as $N_f = P_f N$, where N is the total number of pebbles, in our case $N = 5000$. Note that the value of P_f should be properly chosen such that N_f is an integer. P_f is set to 0.02% in our simulations. This corresponds to one crushed pebble out of 5000 pebbles in a unit box, meaning that we define the initiation of failure in the pebble bed, once the first pebble has reached its critical energy.

In the simulations, assemblies of spheres are compressed uniaxially or triaxially by strain loading. When the first pebble fails, the corresponding macroscopic stress σ_z along the loading direction and the average contact force F_{ave} are taken as the load level for failure initiation. A large number of simulations are performed so as to obtain statistical information on the critical load level for failure initiation. Each set of simulations corresponds to one initial configuration of pebble beds. For one set corresponding to one PF, first, uniaxial or triaxial loading is performed for non-crushable pebbles, and after a small load step when the equilibrium state is achieved we take the strain energy of every pebble, the corresponding macroscopic stresses and F_{ave}. Second, each pebble is assigned

Table 1
The mean critical load level for failure initiation with standard deviation (SD) for failure probability of $P_f = 0.02\%$, resulting from 1000 simulations for each PF. In each simulation, 5000 spheres are compressed uniaxially (Uni) or triaxially (Tri).

$N = 5000$, $N_f = 1$		$\overline{F}_{ave}$ (N)	$\overline{\sigma}_z$ (MPa)
Uni	PF ≈ 62.6%	0.450±0.099	2.410±0.568
	PF ≈ 63.4%	0.447±0.099	2.547±0.602
	PF ≈ 64.0%	0.449±0.097	2.752±0.630
Tri	PF ≈ 64.0%	0.518±0.114	2.544±0.583

to a critical energy as described above. Third, we check if there is any pebble crushed, namely $W_a > W_c$, beginning from strain energy data obtained from the initial load step. If one or more pebbles are found to be crushed, then the corresponding macroscopic stresses and F_{ave} are recorded as the load level for failure initiation. If no pebble failed in this step, then the next load step or higher loads are applied until the load level for failure initiation is identified. For one set of simulations, assignments of critical energy are randomly performed 100 times. Consequently, there will be 100 resulting load levels for failure initiation. In other words, a set of simulations include 100 load levels for the same PF. Moreover, for each level of PF as listed in Table 1 ten different initial configurations have been created. Accordingly, there are 1000 load levels for failure initiation for a similar PF.

Table 1 shows the mean values of F_{ave} and σ_z and their standard deviations for several PFs. Note that the distributions of the strength of pebbles in different simulations have been randomly generated leading to the variation of failure initiation load levels even for the same PF. It can be seen from Table 1 that for uniaxial loading the PF has no influence on $\overline{F}_{ave}$ for failure initiation. On the other hand, $\overline{\sigma}_z$ becomes higher with increasing PF, even though $\overline{F}_{ave}$ and $\overline{\sigma}_z$ belong to the same load level. This is possible, since the relation between them depends on the PF, as has been shown in the discussion of Fig. 6. The loading method (uniaxial, triaxial) has an influence on both $\overline{F}_{ave}$ and $\overline{\sigma}_z$. Compared to the uniaxial loading for the same PF(≈64.0%), $\overline{F}_{ave}$ for triaxial loading is significantly higher, but the stress which is the same along either axial or lateral direction decreases to some extent.

The distribution of σ_z for a PF≈64.0% resulting from uniaxial loading is shown in Fig. 8. There are ten sets, corresponding to ten different initial configurations with approximately the same PF≈64.0%. The probability estimator $P(x_i) = i/(N+1)$ is used here where x_i is the ith load level in an ascending sequence of all load levels obtained from the simulations. One can see that failure initiation could start under a small load level, and the load levels are distributed in a wide range, i.e., σ_z ranges from 1 to 4.6 MPa. Compared with the previous investigation [3] which used directly the crush test data and the failure criterion based on inter-granular forces, the current study provides more detailed information on the actual load distribution associated with failure initiation, as shown in Fig. 8.

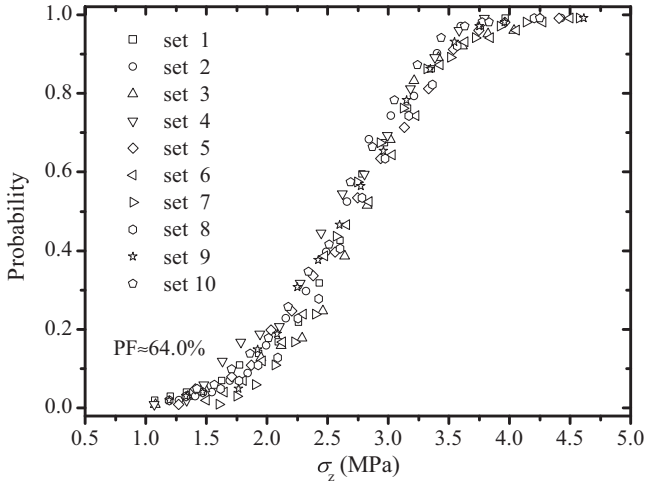

Fig. 8. Distribution of load levels for $P_f = 0.02\%$. σ_z is the macroscopic stress along the loading axis for uniaxial loading. There are 100 obtained load levels for each set.

According to our principle approach, the critical load level is defined to being reached, once the first pebble fails. In practice, the strain loading is applied gradually and checking all pebbles for failure, i.e., $W_a > W_c$, is made after each load step when the assembly of pebbles has reached an equilibrium state. Although each load step has been chosen small, it was sometimes found that more than one pebble is crushed after a load step. This means the derived load level for $P_f = 0.02\%$, i.e., crushing of the first pebble, is slightly overestimated.

3.3. Discussion of both methods

In the numerical-analytical method, for any prescribed P_f it is easy to obtain the corresponding load level in terms of either F_{ave} or σ from Figs. 5 and 6. The load level predicted in this method is kind of an average value with unknown error band. Moreover, the validity of this method highly depends on the assumption that the strain energy distribution among pebbles is not influenced by the failure of pebbles. This assumption may not be valid when many pebbles are crushed. However, the method does not offer a possibility to detect when the assumptions will be violated. In this sense, P_f defining the failure initiation has to be very small for the numerical-analytical method.

In the numerical method, failure initiation means per definition that $N_f = P_f N$ pebbles have failed. In particular, as we define the crushing of the first pebbles as the failure initiation, the underlying DEM simulations are more accurate than the predictions by the numerical-analytical method. Furthermore, this method gives not only a single value for failure initiation, but more information in the form of the distribution of the load level (see Fig. 8). However, the disadvantage of this method that it is more computational expensive.

For a failure probability $P_f = 0.02\%$, the predicted load level using the numerical-analytical method is $F_{ave} = 0.466$ N for uniaxial loading, and $F_{ave} = 0.549$ N for triaxial loading. Both of them are slightly higher than the corresponding values reported in Table 1. According to Fig. 6, $F_{ave} = 0.466$ N corresponds to a uniaxial pressure of about 2.5 MPa for various PFs. As will be discussed later, the overall stress–strain relation will not be influenced until a uniaxial pressure of about 4 MPa, which means that there will be a fraction of pebbles which have already been crushed during loading while it cannot be realized from the overall stress–strain curves.

4. Modeling of failure propagation in a pebble bed

According to Fig. 8, pebbles may fail even under a very small load level. Consequently, the failure of pebbles is almost unavoidable during mechanical loading. Hence, it is essential to study, in addition to failure initiation, the influence of failure propagation on the macroscopic response. For example, it is of concern from which fraction of crushed pebbles on the macroscopic stress–strain relation will be influenced.

4.1. Characterization of crushed pebbles

To begin with, two assumptions are made in this work about, first, the shape of crushed pebbles and, second, their critical energy after a crushing event. As for the shape of crushed pebbles, different failure forms of Li_4SiO_4 pebbles have been found in crush test [13].

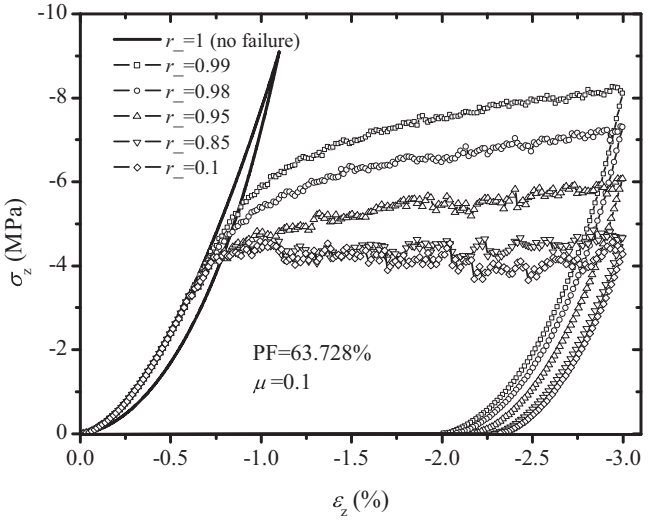

Fig. 9. Influence of reduction ratio on the stress–strain relation along the loading axis for uniaxial loading.

In this work it is assumed that the crushed pebbles still have a spherical shape but with a smaller size. A reduction ratio r_-, defined as the ratio of pebble size after and before failure, is introduced. The ratio has to be chosen in advance from a range from 0 to 1. $r_-=0$ corresponds to the case that crushed pebbles are removed, and $r_-=1$ corresponds to the case that no failure of pebbles occurs in pebble beds. As for the critical energy for crushed pebbles, it is assumed to be the same as before failure. In this way, we allow for pebbles to fail several times during loading.

Obviously, the proposed method of size reduction for crushed pebbles violates mass conservation. However, in this study which provides a first attempt to investigate failure propagation inside pebble beds using a simplified model, this seems to be acceptable in view of the following aspects: First, we do not consider any physical inertia effects. Second, removing mass from the simulation by the reduction of the radius and, thus, by reduction of the volume, corresponds to the assumption that the part of the crushed pebble removed no longer contributes to the force chains, and thus can be neglected in the DEM simulations.

4.2. Simulation results

Fig. 9 shows the influence of the reduction ratio r_- on the macroscopic stress–strain relation for uniaxial loading. Strain load is applied in small increments (increase 0.0015% per step) up to 3%, from which point on unloading takes place. Even if the size of crushed pebbles is slightly reduced, such as $r_-=0.99$, the stress–strain relation changes significantly compared to $r_-=1$ meaning pebbles are non-crushable. A large r_- can represent a failure form where a small fragment of the pebble peels off. It can be seen that the pebble assembly can sustain more load for a big r_- with increasing strain. On the other hand, a stress plateau is reached beyond a strain of about 0.7% for a r_- less than 0.85. It is found that for a small r_- like 0.1 the crushed pebbles will not fail again, or even have no contacts at all after failure. Their presence does not contribute to the force chains in the pebble bed, and so the macroscopic stress will not be influenced by them. Therefore, the stress–strain response, i.e., the stress plateau, should be independent of the crushed pebbles for small r_-. It is expected that this plateau will exist for the limit case $r_-=0$ when crushed pebbles are removed completely, which is in agreement with the finding by [16,10]. Note that the stress plateau for a smaller r_- found in our simulations will not last forever with increasing strain in laboratory

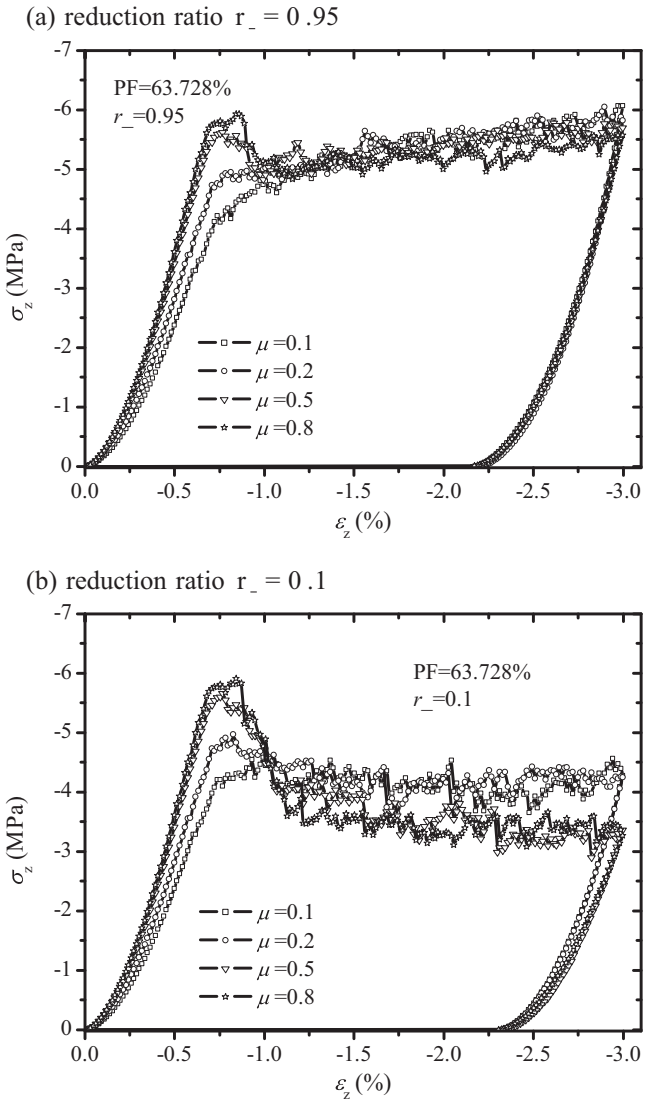

Fig. 10. Influence of the friction coefficient between pebbles on the macroscopic stress–strain relation along the loading axis for uniaxial loading: (a) reduction ratio $r_-=0.95$ and (b) reduction ratio $r_-=0.1$.

compression experiments as, other than assumed in the previous subsection, the fragments of crushed pebbles will actually still stay in the pebble bed. This means they eventually can carry load (contact forces) again when the macroscopic strain gets very large.

In the following analysis, $r_-=0.95$ and $r_-=0.1$ will be considered which correspond to that either a small fragment of the pebble peels off or that crushed pebbles have no influence on the stress–strain relation, respectively. Fig. 10(a) and (b) shows the influence of the friction coefficient between pebbles. For both reduction ratios, a large friction coefficient μ gives rise to a high peak stress before the stress plateau. However, the peak stress almost stays the same for $\mu > 0.5$. For $r_-=0.95$, the stress plateau following the stress peak becomes independent of the friction coefficient for a large strain. For $r_-=0.1$, the stress plateau also appears after the stress peak, but it divides into two scenarios, one for smaller friction coefficients and the other for larger friction coefficients.

Fig. 11(a) and (b) shows the influence of the PF on the stress–strain relation along the loading axis. For both $r_-=0.95$ and 0.1, a higher initial PF leads to a larger stress at small strains. The unloading curves show the same stiffness for different initial PFs. For $r_-=0.1$, different PFs give the same stress plateau which begins at different strain values. There is no stress plateau found

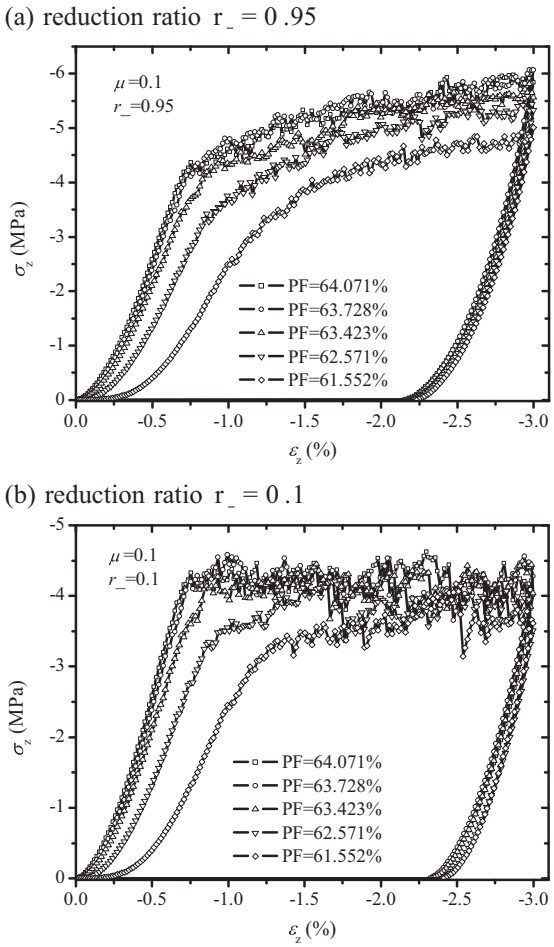

Fig. 11. Influence of the initial packing factor on the macroscopic stress–strain relation along the loading axis for uniaxial loading: (a) reduction ratio r_-=0.95 and (b) reduction ratio r_-=0.1.

for r_-=0.95 since the crushed pebbles can still carry contact forces although their force-carrying ability will decrease. Consequently, the macroscopic stresses can increase with increasing strains for r_-=0.95. On the other hand, crushed pebbles have no contribution to the force chains for r_-=0.1. During unloading, the same stiffness leads to the same stress–strain curve. Note that the unloading curve reflects the elastic deformation of pebble beds.

It is of interest to know how large a fraction of crushed pebbles is needed to affect the macroscopic stress–strain relation. Whether crushed pebbles have an influence on this relation can be characterized by introducing a critical difference between the stresses for crushable and non-crushable pebbles at the same strain. The critical difference has to be defined reasonably small. For example, we may set the critical difference to be 5%. For PF = 64.071% in Fig. 11(a), i.e., r_-=0.95, we counted the crushing of 11 pebbles during loading to ε_z = 0.67% or σ_z = 4.02 MPa where the stress difference at the same strain reaches 5%. This corresponds to a fraction of 0.22% pebbles crushed. For the same PF and a reduction ratio of r_-=0.1 in Fig. 11(b), when the critical difference has reached 5% there have been 10 pebbles crushed with a loading level of ε_z = 0.67% or σ_z = 4.0 MPa. In this case the fraction of crushed pebbles has to be less than 0.2% in order not to influence the macroscopic stress–strain relation. For a low initial PF = 61.552% in Fig. 11(a) and (b), for both r_-=0.95 and 0.1 the crushing of 5 pebbles corresponding to a fraction of 0.1% of crushed pebbles during loading up to ε_z = 1% or σ_z = 2.5 MPa will lead to reaching the critical difference of 5%. It can be seen that the fraction of crushed pebble below which the macroscopic stress–strain is not influenced depends on PF while it is independent of the reduction ratio r_-. This conclusion is meaningful for practical application. For pebble beds subjected to compression test the macroscopic stress–strain relation can be measured. This relation can also be calculated from DEM simulations. Both relations should agree for small load levels. When the critical difference between the relations is reached, the fraction of crushed pebble can be estimated.

Table 2
Statistical information on the number of center points of crushed pebbles falling into one of 27 sub-boxes. N_f crushed pebbles are found during loading up to the maximum strain of 3% for PF = 63.728 and μ = 0.1.

r_-	N_f	N_f/27	SD[a]	SD[b]
0.95	528	19.6	4.11	(2.49, 6.39)
0.1	269	9.96	3.44	(1.83, 4.64)

[a] SD for DEM simulations.
[b] For purposes of comparison: minimum and maximum SD for N_f points generated randomly 2000 times.

4.3. Spatial distribution of pebble failure

The overall stress–strain responses, as shown in Figs. 9–11, present instabilities due to crushing events of pebbles. For pebble beds with multi-sized spheres subjected to uniaxial loading, localization of crushing of spheres has been observed by [16]. Other than in the work presented here, a stress-dominated failure model and rigid wall conditions have been used for the DEM simulations on sphere crushing by [16]. If there would also be a localization of crushed pebbles in our case, the mechanical and thermal properties of the region where localization takes place could be significantly modified compared to the properties of the bulk. Therefore, it is beneficial to know the distribution of the position of crushed pebbles. In this work, we characterize the distribution of the position of crushed pebbles statistically.

At first, the cubic unit box containing all pebbles is divided into 27 equal cubic "sub-boxes" like a classic Rubik's cube. The number of crushed pebbles found in each sub-box is counted according to their center points. The mean number of crushed pebbles in each sub-domain is N_f/27, and the standard deviation (SD) indicates the scatter of their positions. A small SD denotes that crushed pebbles are distributed uniformly. Table 2 shows the statistical information of crushed pebbles.

In order to be able to judge if the SD for crushed pebbles is small or big, additionally N_f points are generated randomly in a unit box corresponding to the unit cell of the DEM simulations, such that the points satisfy a uniform distribution. Then, the number of such points falling in each sub-box is counted. 2000 SDs are derived by generating N_f points 2000 times. The minimum and maximum values are shown in Table 2 for comparison. One can see that the SD for crushed pebbles lies between the minimum and maximum one for uniform distributions, meaning that the distribution of the position of crushed pebbles is fairly uniform. Thus we can conclude that localization of crushed pebbles does not happen.

5. Conclusions

The influence of pebble failure on the overall response of pebble beds subjected to mechanical loading is investigated in this work. The pebble strength used in this work is derived from Li_4SiO_4 pebbles from the batch OSi 07/1. Failure initiation is studied with both a numerical-analytical and a numerical method. According to the results from both methods, failure initiation can occur under load levels with low compressive stresses. In particular, if failure initiation is defined as soon as 0.02% of the pebbles have crushed, this corresponds to a uniaxial pressure of about 2.5 MPa. Therefore,

the subsequent failure propagation is studied by introducing a reduction ratio for the size of crushed pebbles. A slight reduction of the size of pebbles after crushing, such as r_{-}=0.99, will greatly influence the overall stress response of the pebble bed. Below a certain reduction ratio, $r_{-} \leqslant 0.85$, the stress–strain relation is hardly influenced by crushed pebbles and a stress plateau appears. For various reduction ratios, the unloading stiffness is almost the same. Moreover, the influence of the friction coefficient and packing factor is also discussed. A higher friction coefficient leads to a larger peak stress before the stress plateau. A lower packing factor leads to a more compliant stress response at the same strain level. Finally, it is found that there is no significant localization of crushed pebbles during failure propagation.

Acknowledgements

This work is supported by the scholarship program CSC-HGF (China Scholarship Council (CSC) and Helmholtz Association of German Research Centres (HGF)) and the programme FUSION of Karlsruhe Institute of Technology (KIT). This work has been carried out at Institute of Applied Materials (IAM, former IMF II) of KIT.

References

[1] L. Giancarli, M. Ferrari, M. Fütterer, S. Malang, Candidate blanket concepts for a European fusion power plant study, Fusion Engineering and Design 49–50 (2000) 445–456.
[2] Y. Poitevin, L. Boccaccini, A. Cardella, L. Giancarli, R. Meyder, E. Diegele, R. Laesser, G. Benamati, The European breeding blankets development and the test strategy in ITER, Fusion Engineering and Design 75–79 (2005) 741–749.
[3] Y. Gan, M. Kamlah, H. Riesch-Oppermann, R. Rolli, P. Liu, Crush probability analysis of ceramic breeder pebble beds under mechanical stresses, Journal of Nuclear Materials 417 (1–3) (2011) 706–709.
[4] P. Cundall, O. Strack, A discrete numerical model for granular assemblies, Geotechnique 29 (1) (1979) 47–65.
[5] Z. An, A. Ying, M. Abdou, Application of discrete element method to study mechanical behaviors of ceramic breeder pebble beds, Fusion Engineering and Design 82 (15–24) (2007) 2233–2238.
[6] Z. An, A. Ying, M. Abdou, Numerical characterization of thermo-mechanical performance of breeder pebble beds, Journal of Nuclear Materials 367–370 (Part 2) (2007) 1393–1397.
[7] Y. Gan, M. Kamlah, Discrete element modelling of pebble beds: with application to uniaxial compression tests of ceramic breeder pebble beds, Journal of the Mechanics and Physics of Solids 58 (2) (2010) 129–144.
[8] Z. Lu, A. Ying, M. Abdou, Numerical and experimental prediction of the thermomechanical performance of pebble beds for solid breeder blanket, Fusion Engineering and Design 49–50 (2000) 605–611.
[9] A. Ying, H. Huang, M. Abdou, Numerical simulation of ceramic breeder pebble bed thermal creep behavior, Journal of Nuclear Materials 307–311 (Part 1) (2002) 827–831.
[10] G. Marketos, M. Bolton, Quantifying the extent of crushing in granular materials: a probability-based predictive method, Journal of the Mechanics and Physics of Solids 55 (10) (2007) 2142–2156.
[11] K. Tsuchiya, H. Kawamura, S. Tanaka, Evaluation of contact strength of Li_2TiO_3 pebbles with different diameters, Fusion Engineering and Design 81 (8–14) (2006) 1065–1069.
[12] N. Zaccari, D. Aquaro, Mechanical characterization of Li_2TiO_3 and Li_4SiO_4 pebble beds: experimental determination of the material properties and of the pebble bed effective values, Fusion Engineering and Design 82 (15–24) (2007) 2375–2382.
[13] S. Zhao, Multiscale modeling of thermomechanical properties of ceramic pebbles, PhD Thesis, Karlsruhe Institute of Technology (KIT), 2010.
[14] R. Knitter, Quality control of lithium orthosilicate pebbles and long-term annealing behaviour of ceramic breeder materials, Report on TW2-TTBB-002b-D2, FZK FUSION Nr. 220, 2003.
[15] S. Zhao, Y. Gan, M. Kamlah, T. Kennerknecht, R. Rolli, Influence of plate material on the contact strength of Li_4SiO_4 pebbles in crush tests and evaluation of the contact strength in pebble-pebble contact, Engineering Fracture Mechanics (2012), http://dx.doi.org/10.1016/j.engfracmech.2012.05.011. http://www.sciencedirect.com/science/article/pii/S0013794412002135?v=s5
[16] G. Marketos, M. Bolton, Compaction bands as observed in DEM simulations, in: Proceedings of the 5th International Conference on Micromechanics of Granular Media, Powders and Grains, 2005, pp. 1405–1409.